THE EFFECT OF DUCTILE CRACK EXTENSION ON CLEAVAGE FRACTURE PROBABILITY.

A. Martín-Meizoso*, I. Ocaña-Arizcorreta†, J. Gil-Sevillano†, M. Fuentes-Pérez*

In the ductile-to-brittle transition zone of steels, ductile crack extension occurs prior to unstable cleavage cracking. This paper studies the effect of such stable crack propagation on the brittle toughness probability value by means of a statistical fracture model based on microstructural parameters. The model predicts a substantial increase of the fracture probability for a given load condition (fixed by the J or K level) when some propagation occurs relative to the static, non propagating crack case. The model assumes brittle fracture to occur when a ferrite grain size microcrack -conditioned to the propagation of a slip-induced carbide size microcrack- is able to propagate into the neighbouring grains. The results show reasonable agreement with the fracture statistics of a SA 533B c.1 bainitic steel.

INTRODUCTION

Steel fractures at the brittle-ductile transition zone initially take place by void coalescence (ductile mode) and then change to cleavage (brittle and catastrophic fracture mode). Ductile crack extension increases with temperature. At high enough temperatures, the ductile crack propagation extends throughout the fracture surfaces without brittle zones. It is also observed that ductile extension scatter increases with temperature.

Figure 1.c sketches the plastic zone development during the load process. Until reaching the material critical stress intensity factor, there is no tearing of the blunting crack tip, and the plastic zone grows pinned to the crack tip. Above this critical value, K_{IC}, ductile crack extension takes place and, so, the plastic zone samples virgin volumes of material. Intentionally, in Fig. 1.c, the plastic zone size

(*) Centro de Estudios e Investigaciones Técnicas de Guipúzcoa (CEIT), P°. Manuel de Lardizabal, 15, 20009-San Sebastián, Guipúzcoa, Spain.
(†) Escuela Superior de Ingenieros de San Sebastián. Universidad de Navarra, Apartado 1674, 20080-San Sebastián, Guipúzcoa, Spain.

has been sketched increasing its size in a parabolic way. Assuming a constant tearing modulus, T (in terms of K: T = dK/da), for the material, the applied stress intensity factor increases linearly with crack extension, Δa, and then the plastic zone size will increase in a parabolic way.

THEORETICAL MODELLING

Figure 1.a shows how the problem is faced in the context of the computer programme developed at CEIT for brittle toughness predictions. The programme develops a probabilistic model based on the weakest link concept and a detailed account of it has already been published (1-4). Computations are accurate provided that crack tip ductile tearing does not take place. After crack tip tearing, ductile crack extension takes place, as depicted in Fig. 1, and, so the advancing plastic zone samples new volumes of material. Computations according to Fig. 1.a should then be regarded as a lower bound for actual brittle fracture probability. The target of this contribution is to estimate the effect of these additionally scanned volumes on the cleavage fracture probability when stable crack propagation occurs prior to cleavage (i.e., in the ductile-to-brittle transition zone).

Although it was already obvious in the formulation proposed by Pineau-Beremin (5-7), Wallin (8) showed explicitely that any toughness modelling of a statistically homogeneous material based on

i) the weakest-link hypothesis and,

ii) which assumes stress and strain fields geometrically similar around the crack tip scaling with the J integral (or K_I^2) for distances,

predicts two parameter Weibull functions for toughness distribution, with modulus m = 2 (distributions of J_C or CTOD) or m = 4 (for distributions on K_{IC}):

$$F(K_{IC}) = 1 - \exp(-B \cdot K_{IC}^4 \cdot \Psi) \qquad (1)$$

where F stands for the toughness distribution function (in terms of K_{IC} in this case), B is the crack front length and Ψ is a material parameter dependent on temperature, strain rate and tested geometry. A rigorous explanation, with a detailed description of the hypothesis and a discussion about the results of these models resulting on equation (1) has been done by Slatcher (9).

Figure 1.d represents an upper bound for the cleavage fracture probability. This -larger than real- volume may be decomposed in Fig. 1.a (lower bound, already computed) and an additional volume obtained by scanning the plastic zone over a length Δa.

To compute the cleavage fracture probability in the actual case after crack tip tearing, Fig. 1.c, an upper and lower limit were devised according to Figs. 1.b and 1.d. Figures 1.b and 1.d may be decomposed in "static" plastic zones and "scanned" areas. Figure 2 shows how Figs. 1.d and 1.b are decomposed to compute the cleavage failure probability. The zone labeled A is the final plastic zone extension, its cleavage failure probability was computed by the previous (static) version of the programme. The scanned area, B, is discretized in horizontal strips that will be considered of uniform effective (for cleavage fracture) stress. As a first approximation, the maximum principal stress, σ_1, at a given strip height, y, will be used as the cleavage fracture effective stress. Figure 3 is a normalized representation of the locus of 1 MPa maximum principal stress according to the HRR elasto-plastic stress field solution (10-13) for a material with a non-linear elastic behaviour of Hollomon-type,

$$\varepsilon = \varepsilon_0 \left(\frac{\sigma}{\sigma_0} \right)^n \qquad (2)$$

where σ stands for the von Mises equivalent stress, ε is the work-equivalent plastic strain, σ_0 and ε_0 are, respectively, the 0.2% yield stress and strain (= 0.002), and n is the hardening exponent. The hardening exponent used in Figs. 3 and 4, n = 5.3, was obtained by fitting to the experimental behaviour of the material in the temperature range from -40 to -70°C (3).

Clearly, from Fig. 3, the maximum principal stress at a given height is found at about an angle of 45° with respect to the crack propagation plane (it slightly depends on the strain hardening exponent, n). According to the accepted evidence and the proposed cleavage modelling (1-4), cleavage fracture nucleation in steels is slip-induced, so, dislocations are required to move in order to trigger fracture. Thus, nucleation will only take place within the plastic zone. Figure 4 plots the normalized plastic zone boundary (computed from the HRR elasto-plastic stress field solution (10-13)). Whenever the maximum principal stress, for a given height, lies within the elastic zone (outside the plastic zone), the principal stress at the elasto-plastic boundary is used there to compute the cleavage failure probability instead of the maximum principal stress for this height.

RESULTS

Experimentally measured microstructural and mechanical parameters of a bainitic steel, S A533B C.1, from a previous study (3) have been used in the calculations. Material strain hardening exponents are: n = 5.29 and n = 5.30 at -40 and -70°C, respectively. Two large sets of K_{IC} data for brittle fracture propagation computed from J integral values measured with CT specimens 25 mm thick at -40°C and -70°

C, mainly after some stable crack propagation were also available. Figure 5 summarizes the experimental cleavage fracture data in the form of a Weibull plot. Figures 6.a and b show the cleavage results vs. the prior stable propagation, i.e., the resistance curve (R curve: K_I versus Δa) at both temperatures being studied. Maximum ductile crack propagations up to 200 and 1000 μm at -70°C and -40°C, respectively, were recorded. Solid circles in Figs. 6.a and b are the toughness values for which the probabilities of cleavage have been calculated with the model.

The microstructural parameters (carbide and grain size distributions), mechanical properties (Young's modulus, material strain hardening exponent versus temperature) and local -micromechanism related- fracture parameters (arresting ability of the different interfaces between carbide/ferrite and ferrite/ferrite and carbide failure probability parameters) used in the calculations are those reported previously for cleavage failure predictions from notches or non-propagating cracks (1-4).

Figures 7.a and 7.b summarize the model predictions at -70°C and -40°C, respectively, with and without ductile crack extension and according to Figs. 1.b and d (lower and upper cleavage fracture probability bounds). For Fig. 1.b computations, 20 steps were used to discretize the ductile crack propagation. Note that both upper and lower boundaries coincide until crack tip tearing takes place. The subsequent ductile crack extensions (in accordance with Figs. 6.a and b) are labelled in Figs. 7.a and 7.b.

Figure 8 summarizes the lower bound computations at -70°C and -40°C. The model predictions agree qualitatively with several experimental findings: an upwards kink on the toughness probability is predicted at the onset of stable crack propagation and the general effect of stable crack propagation is to increase the Weibull modulus above the theoretical value of 4 in the transition region. The quantitative disagreements on the scale parameter of the Weibull distributions are ascribed to an increase of the arrest capabilities of the microstructural boundaries and a decrease in nucleation probability from carbides as temperature increases.

CONCLUSIONS

1. Ductile crack extension plays a very significative role on cleavage fracture probability.

2. Even when ductile crack extension, Δa, is small compared to the plastic zone size, cleavage fracture probability increases due to the larger volume sampled at the maximum stresses.

3. The largest effect is found soon after the beginning of the crack tip tearing. With

larger crack extensions, again a Weibull modulus of 4 is asymptotically attained, now with larger cleavage fracture probabilities.

4. The attempted model predicts reasonably well the experimentally observed changes in slopes (on a Weibull plot) at the beginning of crack tip tearing.

ACKNOWLEDGMENTS

The contents of this contribution are consequence of a C.E.C.A. Project (D.G. XII, ECSC "Steel programme," project number 7210/KA/934-91-F1.03a). One of the authors (I.O.A.) gratefully acknowledges the grant from the Departamento de Educación, Universidades e Investigación of the Basque Government, (Vitoria-Gazteiz). The authors would like to thank Segunda Pérez-Paz for drawing the figures.

LIST OF SYMBOLS

a = Crack size (m)
B = Crack front length (m)
CTOD = Crack tip opening displacement (m)
E = Young's modulus (MPa)
F = Cumulative toughness distribution function
J = J integral (kJ/m^2)
J_C = Critical J integral (kJ/m^2)
K_I = Mode I stress intensity factor (MPa$\sqrt{m}$)
K_{IC} = Critical stress intensity factor (MPa$\sqrt{m}$)
m = Weibull modulus (shape parameter)
n = Strain hardening exponent
R = Ductile resistance curve (kJ/m^2)
T = $dK/d\Delta a$ = Tearing modulus (MPa/$\sqrt{m}$)
x = horizontal distance from the crack tip (m)
y = vertical distance to the crack plane (m)
Δa = Crack growth (m)
ε = work-equivalent plastic strain
ε_0 = 0.2% yield strain
σ = von Mises equivalent stress (MPa)
σ_0 = 0.2% yield stress (MPa)
σ_1 = maximum principal stress (MPa)
Ψ = material constant dependent on temperature

REFERENCES

(1) A. Martín-Meizoso, R. García-Arrizabalaga, J. Gil-Sevillano, "Fracture

Behaviour and Design of Materials and Structures", D. Firrao, ed., EMAS, London, Vol. 1, Turin, 1990, pp. 70-74.
(2) J. Gil-Sevillano, A. Martín-Meizoso and M. Fuentes-Pérez, Anales de Mecánica de la Fractura, Vol. 8, 1991, pp. 3-8.
(3) C.E.I.T., "Tenacidad de un acero para recipientes a presión (A 533B C.1) en la zona de transición dúctil-frágil. Predicción del límite de propagación estable de la grieta", Final report, CECA project No. 7210/KE/931, 1991, F5-5/87.
(4) A. Martín-Meizoso, I. Ocaña-Arizcorreta, J. Gil-Sevillano, M. Fuentes-Pérez, "Modelling Cleavage Fracture of Bainitic Steels", Acta Metall. Mater., in press (1994).
(5) A. Pineau, "Advances in Fracture Research", Vol. 1, D. Francois, ed., Pergamon Press, Oxford, 1981, pp. 179.
(6) F. M. Beremin, Metall. Trans. A., Vol. 14A, 1983, pp. 2277.
(7) D. Qu, X.W. Wang, C.K. Tsai, "Mechanical Behaviour of Materials - IV", Vol. 2, J. Carlsson and N.G. Ohlson, eds., Pergamon Press, Oxford, 1984, pp. 779.
(8) K. Wallin, Eng. Fracture Mechanics, Vol. 19, N. 6, 1984, pp. 1085-1093.
(9) S. Slatcher, Fatigue Fract. Eng. Mater. Struct., Vol. 9, 1986, pp. 275.
(10) J. W. Hutchinson, J. Mech. Phys. Solids, Vol. 16, 1968, pp. 13-31.
(11) J. R. Rice and G. F. Rosengren, J. Mech. Phys. Solids, Vol. 16, 1968, pp. 1-12.
(12) J. W. Hutchinson, J. Mech. Phys. Solids, Vol. 16, 1968, pp. 337-347.
(13) C. F. Shih, "Tables of Hutchinson-Rice-Rosengren Singular Field Quantities", Material Research Laboratory, MRL E-147, Brown University, Providence, 1983.

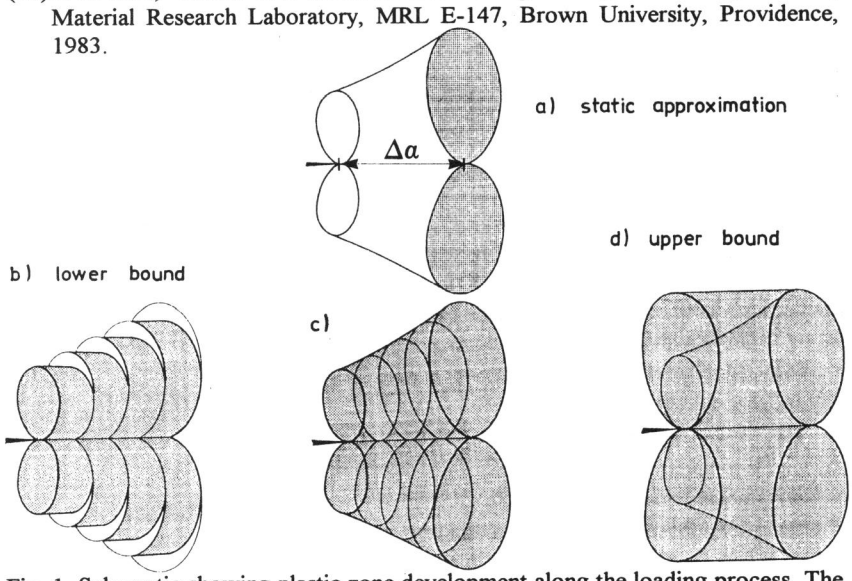

Fig. 1. Schematic showing plastic zone development along the loading process. The shaded areas represent: a) the static approximation, b) a lower bound, c) the actual case, and d) an upper bound.

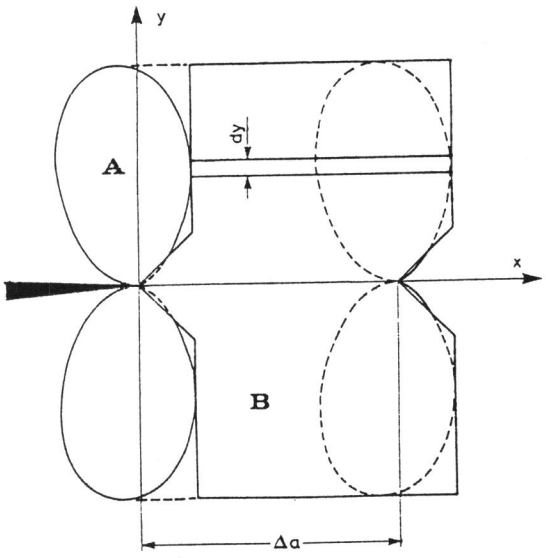

Fig. 2. Scanned plastic zone decomposition used within the computations of the upper and lower bound (according to Figs. 1.b and 1.d).

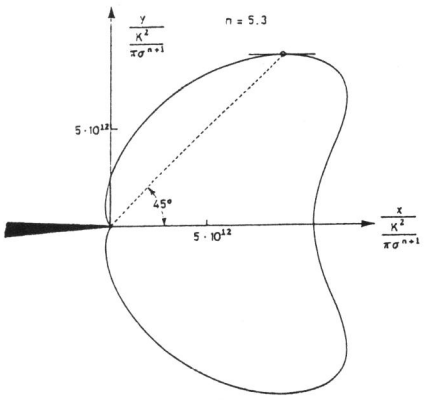

Fig. 3. Locus of 1 MPa maximum principal stress. (H.R.R. elasto-plastic solution (10-13)), n=5.3, normalized non-dimensional length scales.

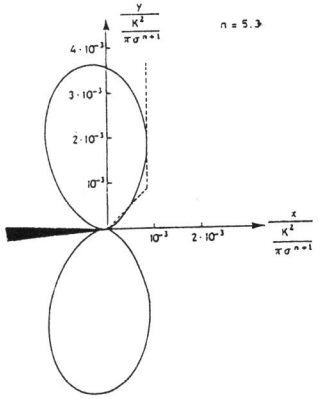

Fig. 4. Plastic zone boundary (H.R.R. elasto-plastic solution (10-13)), n=5.3, normalized non-dimensional length scales.

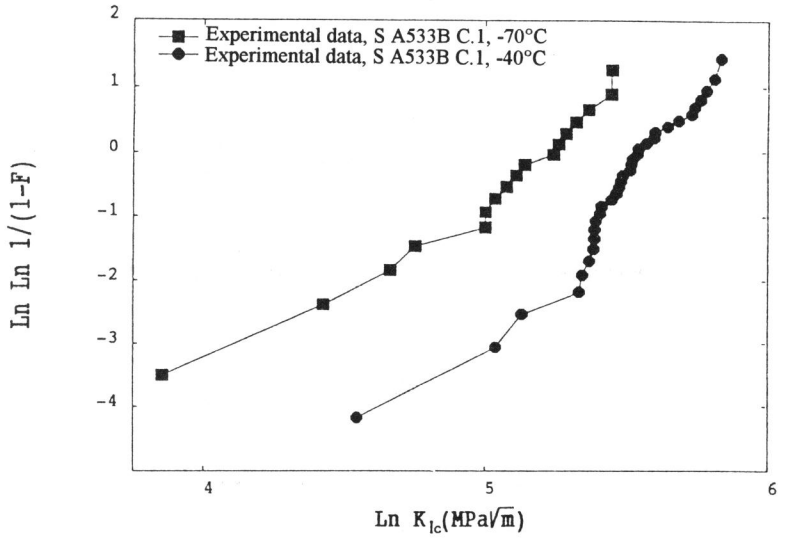

Fig. 5. Experimental results for S A533B C.1 bainitic steel, at -70 and -40°C on a (cumulative failure probabilities) Weibull plot.

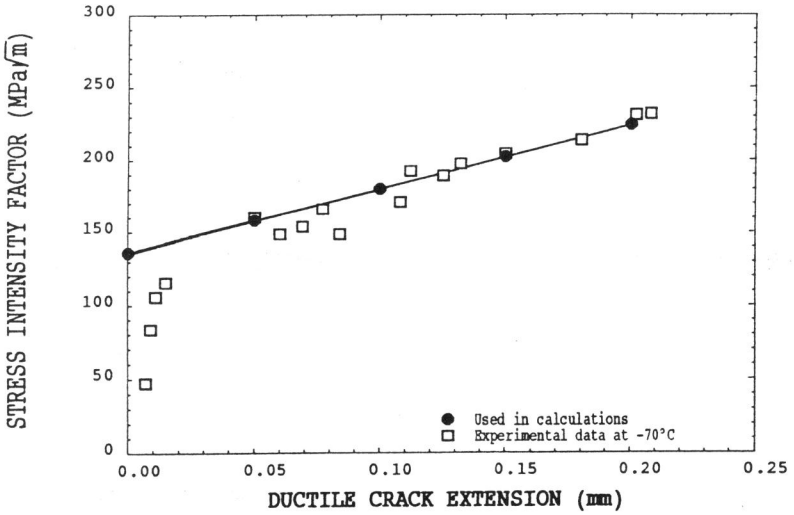

Fig. 6.a. Experimental data of resistance curve (R curve) obtained for S A533B C.1 at -70°C. Solid points stand for the simplified data used in the computations.

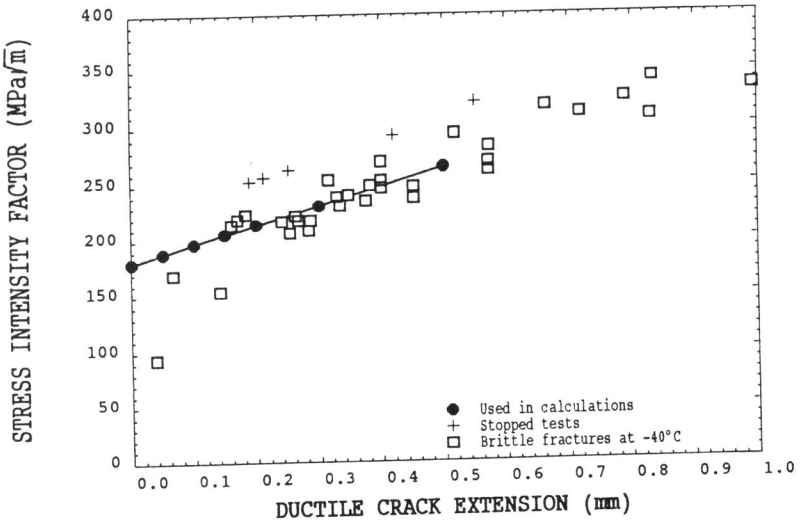

Fig. 6.b. Experimental data of resistance curve (R curve) obtained for S A533B C.1 at -40°C. Solid points stand for the simplified data used in the computations.

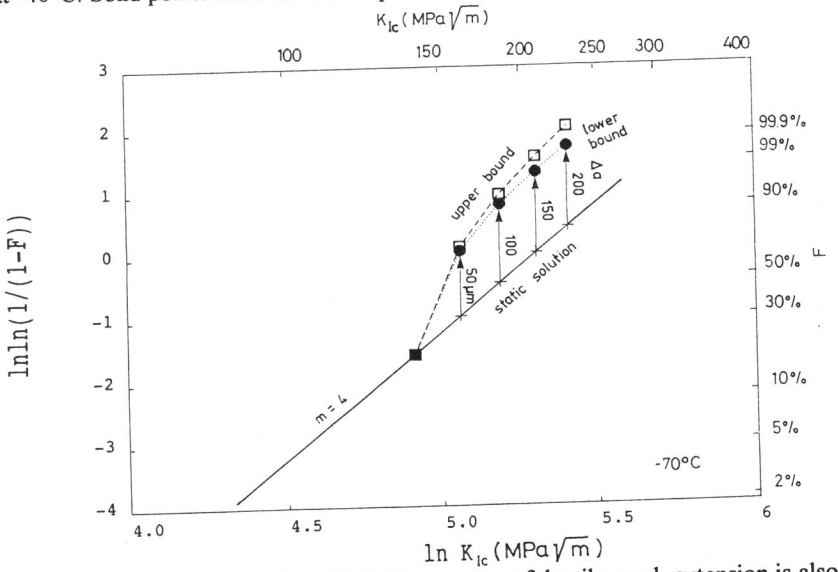

Fig. 7.a. Model predictions for -70°C. The amount of ductile crack extension is also indicated.

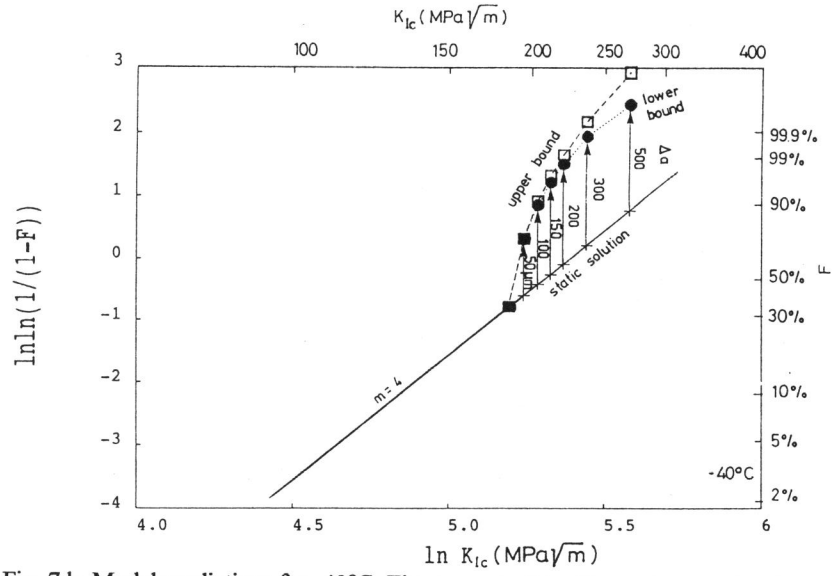

Fig. 7.b. Model predictions for -40°C. The amount of ductile crack extension is also indicated.

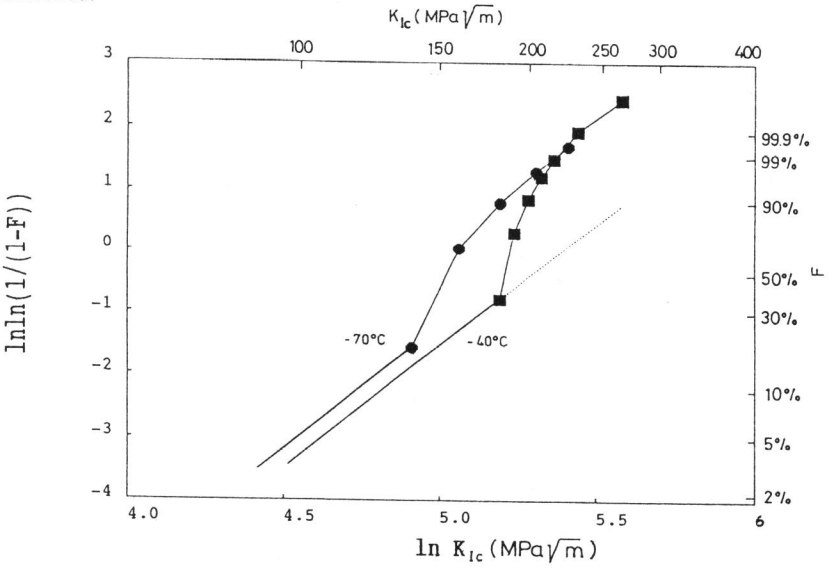

Fig. 8. Lower bound model predictions for -70°C and -40°C cleavage fracture probabilities, on a cumulative Weibull plot.